Materials Science and Technology 30 (2014) 1911-1918

Bearing Steel Microstructures after Aircraft Gas Turbine Engine Service

J. R. Nygaard, M. Rawson, P. Danson, H. K. D. H. Bhadeshia

February 10, 2015

The microstructure of aircraft gas-turbine engine bearing steel has been characterised after service in Rolls-Royce Trent engines, with the focus on the surface condition and the consequences of sliding and rolling contact. The carbide populations at the surfaces of rolling elements are found to be depleted by 30% after 30,000 h engine service. A single ball failure occurred after this period of operation, leading to fatigue spalling that initiated below the contact surface. A comparison between unused bearing raceways and those that have experienced service revealed that the microstructures resulting from secondary hardening remain remarkably stable during operation. Plastic flow along the direction of rolling is confined to a shallow zone $< 2\,\mu$m beneath the contact surfaces. Transmission electron microscopy has revealed a new mechanism of plastic deformation in these bearing steels, in the form of mechanical twinning initiating at interfaces such as prior austenite grain boundaries. It is also demonstrated that work hardening occurs to a depth of some 1 mm in the raceway that has experienced 30,000 h of service.

Introduction

Future aircraft gas-turbine engines seek to operate at greater speeds and temperatures for improved efficiency, leading to increased demands on rolling-element bearings. At 12,500 revolutions per minute a 340 mm bore bearing containing 20 rolling elements will see upwards of 10^{10} stress cycles before an inspection is due. Such gigacycle fatigue conditions should test the stability of bearing steel microstructures [1]. Bearing steels used currently in aircraft gas-turbine engine applications are listed in the first two rows of Table 1. These alloys were derived originally from secondary-hardened tool steels which show greater thermal stability than the 52100 alloy (Table 1) designed for ambient applications [2, 3]. The secondary hardened structures in M50 and M50NiL are not susceptible to the stress-induced material softening [4] or mechanically tempered "dark etching regions" (DER) common in 52100 bearing steel [5]. The absence of DER in the aircraft-grade steels is due to the greater thermodynamic stability of carbides that are rich in Cr, Mo and V when compared with cementite [6]. Typical failure mechanisms in aircraft gas-turbine engine bearings should therefore be different, with surface-initiated failure being the dominating mechanism [7].

Material Selection

Location bearings support the main shaft of an aircraft gas-turbine engine and have M50 steel balls rolling on deep-grooved M50NiL raceways [Fig 1a]. To combat the problem of through fracture in raceways M50NiL was introduced as a low carbon variant of the M50 alloy, enriched with nickel for sufficient fracture toughness to cope with both service stresses and those arising

Table 1: Bearing steel compositions in wt%. The two aircraft-grade alloys are given first [8], followed by the most popular traditional bearing steel for comparison [9]

Steel	C	Mo	Cr	V	Ni	Mn	Si
AISI M50	0.80-0.85	4.0-4.50	4.0-4.25	0.90-1.10	0.10- 0.15	0.15-0.35	0.10-0.25
AISI M50NiL	0.11-0.15	4.0-4.50	4.0-4.25	1.13-1.33	3.20-3.60	0.15-0.35	0.10-0.25
SAE 52100	0.93-1.05	<0.10	1.35-1.60	<0.10	<0.25	0.25-0.45	0.15-0.35

Steel	σ_y (MPa)	σ_{UTS} (MPa)	E (GPa)	Hardness (kg/mm^2)	K$_{IC}$ (MPa$\sqrt{}$m)
AISI M50	2110	2660	219	807	21
AISI M50NiL	2344-1175*	2827-1387*	202	825-500*	16-50*
SAE 52100	1158	2316	210	778	21

Table 2: Bearing steel mechanical properties: the yield strength, ultimate tensile strength, elastic modulus, vickers hardness and fracture toughness respectively. Properties for M50NiL case and core* are both given where possible. Data from [1, 10, 11, 12]

from the fitting process [12, 13, 14]. Whereas M50 can be through hardened, M50NiL is case-hardened in order to retain a high core toughness, Table 2. The introduction of carbon into the surface layers while the steel is in its austenitic condition, followed by transformation into martensite during cooling, is accompanied by a volume expansion that places the surface into compression relative to the core [15]. This compressive residual stress has proven beneficial in retarding fatigue processes [8, 16, 17]. Both the M50 and case-carburised M50NiL require a number of thermal treatments following quenching, including tempering and cryogenic cooling in order to control the level of retained austenite, which can otherwise compromise dimensional stability [18].

The predominant failure mechanism in ordinary bearing steels is rolling contact fatigue (RCF) [19], which describes the accumulation of damage through repetitive contact loading [20]. RCF failures can initiate at inhomogeneities beneath the rolling-contact surface where the shear stress reaches a maximum, or at asperities found on the contact surface itself. Failures culminate in spalling that then leads to further flaking damage which can obscure the initial cause of failure [Fig 1b]. Microstructural changes that occur in the maximally stressed sub-surface region have been well documented in the 52100 steel [21, 22, 23], but less attention has been paid to M50 and M50Nil, particularly in the context of surface fatigue encountered [24]. These are clean steels, produced by vacuum induction melting with vacuum arc remelting (VIM-VAR) to limit oxygen content in the final product [25]. This reduces the non-metallic inclusion content, and hence fatigue initiation sites. As a result, the majority of failures tend to be surface initiated, so the focus of damage has been on tribological aspects rather than structural change [26].

Bearing Design and Application

It is important in damage assessment studies of aircraft gas-turbine engine bearings to identify the position of the contact zone under thrust loaded conditions. As air is taken in at the mouth of the engine it is compressed and ignited with fuel before expanding rearwards providing thrust and driving the turbine blades. This flow of gas causes axial loads along the main shaft which must be supported by bearing design, with the balls positioning themselves further up the raceway groove during motion, away from the central 0° position as illustrated

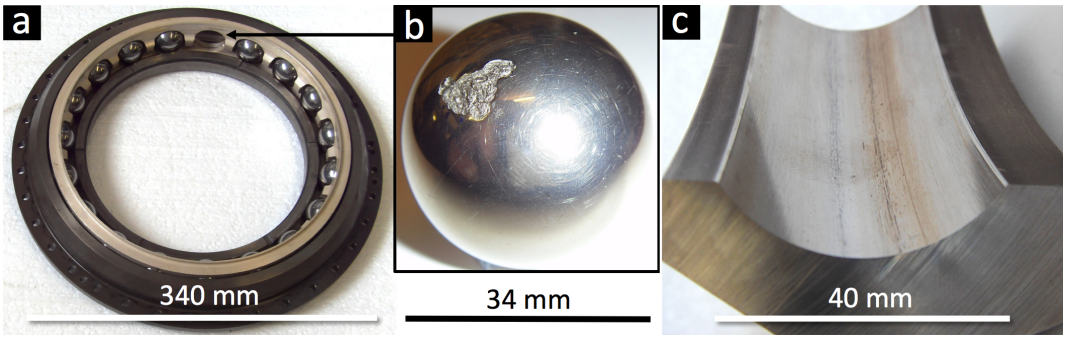

Figure 1: a). Rolls-Royce Trent engine location bearing with inner raceway removed to reveal the rolling elements held within the cage. b). M50 bearing ball removed after 30,000h service displaying a fatigue spall. c) Cross-sectioned M50NiL outer raceway after 30,000h service displaying tracks of discolouration at positions which indicate thrust loading.

in Fig 1c. Individual separation of the balls is maintained by the bearing cage; typically made from 4340 type steel (AMS 6414) and coated with magnesium sulphide or silver plate to address landing wear. Aeroengine bearing failures due to cage damage can arise [27, 28], but in the present fatigue investigation the cage does not feature.

Factors such as the conformity between the ball and raceway curvature affect the size of the contact ellipse under elastic loading, and the stress experienced therein [29, 30]. During aircraft take-off the contact stress between ball and raceway approaches $p_0 = 2\,\text{GPa}$. Assuming classical Hertzian contact, location bearings experience a maximum shear stress $\tau_{max} = 600\,\text{MPa}$ at depths of around 0.2 mm beneath the point of contact. These values only apply for a perfectly lubricated system under full elastohydrodynamic conditions, but the real situation can be more complex. Excessive roughness of the component surfaces [31, 32] or starved lubrication conditions [33, 34] will lead to asperity contact and metal-on-metal traction. Under these circumstances gross sliding can occur within the contact zone and the maximum shear stress shifts towards the contact surface [35]. A high quality surface finish is therefore vital in stopping asperities breaking through the lubricant film. For bearing balls or raceways entering engine service the mean centreline surface roughness value should not exceed $R_a = 0.1\,\mu\text{m}$ [36]. Poly ester-based synthetic lubricants aid in the cooling of location bearings which can experience temperatures approaching 200°C in the aircraft gas-turbine engine. The so-called lambda ratio of lubricant film thickness to composite surface roughness describes friction regimes for bearing operation [37], where a well lubricated system of $\lambda > 1$ is expected for aircraft engine operation. Constant oil circulation is required, during which debris contaminants are actively filtered out to avoid indentation of the components which could initiate surface fatigue failures [24, 38, 39].

Experimental

Rolls-Royce Trent engine location bearings have been examined in the unused condition and following 120 h and 30,000 h running times. The longest running bearing had failed by a single ball spall failure which was examined using fractography. Bearing balls were sectioned using electrode discharge machining, and ground and polished using progressively finer silicon carbide grinding papers followed by polishing with a 1 µm diamond paste and finally a 0.05 µm colloidal silica suspension. Marble's reagent was used to reveal the primary carbides; a solution comprising of 5% copper sulphate to equal parts hydrochloric acid and water. Carbide

Materials Science and Technology 30 (2014) 1911-1918

populations were quantified using image analysis software [40], with microanalysis using energy dispersive X-ray spectroscopy (EDX) on the JEOL 5800LV scanning electron microscope (SEM).

Bearing raceways were sectioned radially and tangentially using a diamond cutting wheel. A mixture of 3% nitric acid and 97% methanol by volume was used as an etchant. In some cases a protective layer of nickel was deposited by sputter coating to preserve the near surface region during grinding. The 0.5 µm sputter layer was deposited at 70mA for ≈10 min. Selected sections were machined using Ga^+ ion milling on the FEI Helios Nanolab focussed ion beam scanning electron microscope (FIB-SEM), and subsequently imaged using the JEOL 200CX transmission electron microscope (TEM). Microhardness was measured on a Mitutoyo MVK-H2 tester using a 200 g load.

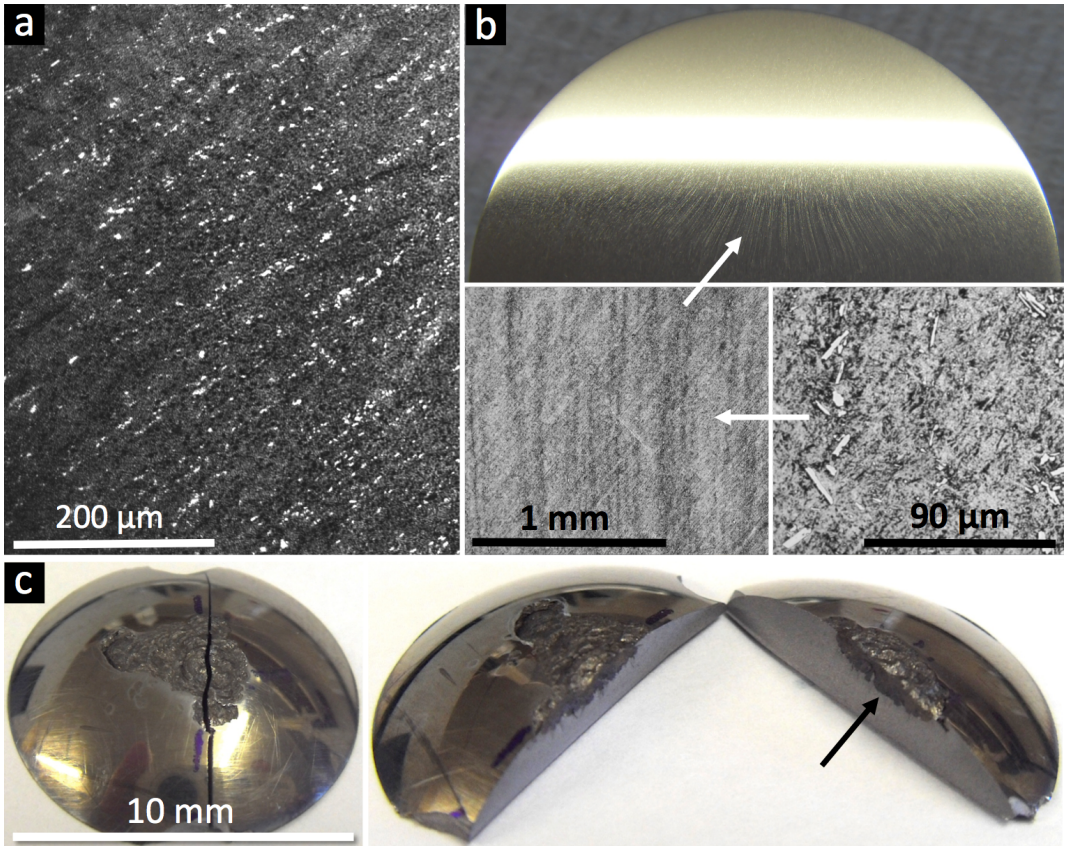

Figure 2: a). M50 bearing ball surface etched to reveal directional primary carbides with bright contrast. b). Cross-sectioned M50 ball interior showing grain flow lines of segregated carbides under optical microscopy. c). Fatigue spall on bearing ball after 30,000 h displays a subsurface crack forcibly opened to reveal a fatigue zone approximately 1 mm in depth (arrowed).

Results and Discussion

M50 bearing balls contain primary carbide stringers at their contact surfaces [Fig 2a], tracing lines of longitude about the spherical components, leading towards two poles at opposite ends of the ball. The stringers permeate throughout the ball interior [Fig 2b], akin to the skins of an onion, and have been cited as the cause for dynamic imbalance in M50 balls [41]. The origin of the stringers is associated with segregation during solidification, which is spread along the length of the bars used as the raw material for the production of balls. This anisotropy in through-hardened balls is referred to as "grain flow" and historically has been blamed for preferential fatigue failures occurring at the polar regions [42, 43, 44].

In the present work, a single ball failure resulted in the discontinuation of the 30,000 h bearing following spalling damage [Fig 1b]. Fractography revealed the fatigue spall had occurred at a location away from the polar regions, so carbide segregation was not thought responsible. Instead, a crack found running through the spall was forcibly opened to reveal a subsurface fatigue zone approximately 1 mm beneath the contact surface [Fig 2c]. The fatigue striations in this zone suggest a subsurface crack initiated fatigue failure, but the exact source could not be identified conclusively.

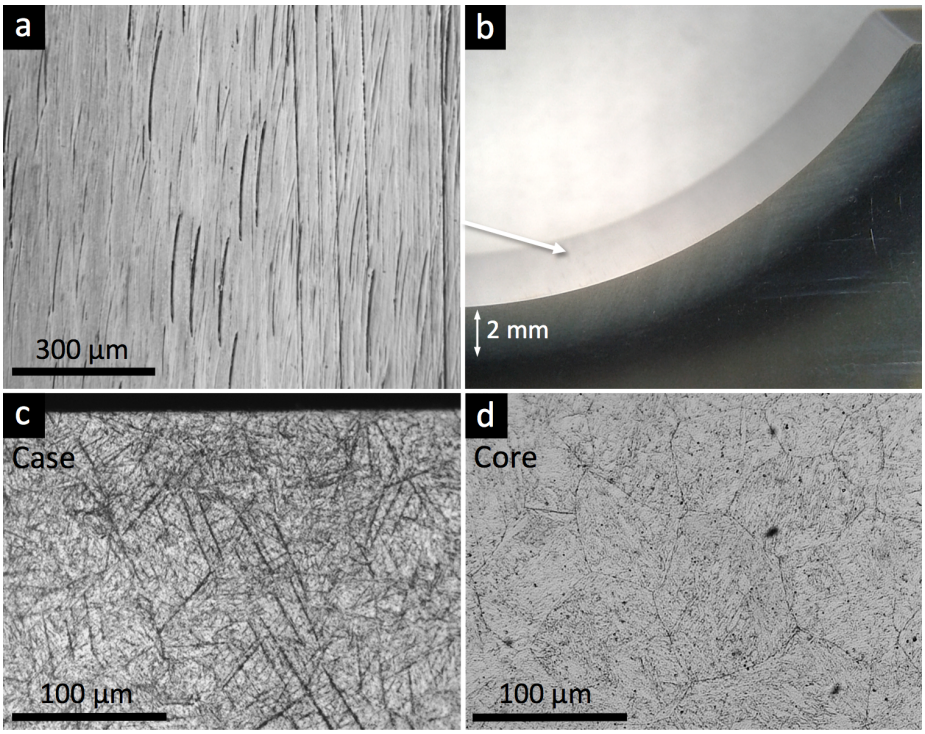

Figure 3: a). Curved scores on the M50NiL raceway after 120 h service caused by ball spinning, (the rolling direction is north to south). b). A cross-section of this M50NiL raceway shows 2 mm deep carburised case after colloidal silica polish. c). Optical micrograph of this high carbon case after etching to reveal plate martensite features. d) The M50NiL core at depths greater than 3 mm shows an etched microstructure of lath martensite with visible prior austenite grains.

M50 primary carbides were characterised by microanalysis, using work by Bridge *et al.*[45] as a reference, confirming the presence of molybdenum rich M_2C type and vanadium rich MC, where 'M' refers to metal atoms. The average primary carbide size was measured as

6.3 µm ± 0.1 µm on the surfaces of the new balls and similarly 6.3 µm ± 0.4 µm on the used balls, but there was greater variation in the number densities found. A 30% decrease in surface carbide population was identified on used balls from the 30,000 h service bearing when compared with the 0 h bearing balls. These post-service observations would suggest precipitate removal under the action of surface shear during rolling contact, however it should be noted that scratches and patches of corrosion on the used ball surfaces may have influenced this apparent reduction in carbide population. Pearson and Dickinson [46] presented evidence of cracked carbides breaking up under surface shear in M50 test bearings. The carbide asperities in their work were found to cause peeling damage at raceway surfaces under low lubrication conditions. Other authors have also reported voids near debonded M50 carbides [47] and separation at the carbide-matrix interfaces [48].

Visual examination of the used M50NiL raceways shows tracks of discolouration which indicate the rolling history of the balls during service. Optical microscopy within these tracks reveals scoring damage and curved indentations caused by ball spinning under thrust loading [Fig 3a]. It is thought that the hard primary carbide asperities on the surfaces of the balls are responsible for such markings. These curved scratches imply a certain amount of sliding takes place within the contact ellipse, and it is this sliding between components that produces a surface shear significant to RCF. Gloeckner and Ebert [35] witnessed similar features under high-speed bearing operation, concluding that sliding shear leads to heat generation, plastic flow and micro-spalling within the contact zone, and hence is a key contributor to surface initiated failures in aircraft gas-turbine engine bearings.

Optical microscopy beneath the raceway surfaces reveals the M50NiL material remains in good condition for all the used bearings examined. The carburised case is densely populated with fine, well-dispersed carbides to a depth of approximately 2 mm [Fig 3b]. Upon etching the high-carbon martensite plates of the case visibly darken [Fig 3c], but much larger features with more irregular morphologies were also encountered here, as shown later in Fig 4. All three raceways exhibited these atypical features within the first 500 µm of their case depth, including the unused bearing. The low carbon microstructure of the M50NiL core resists etching although the prior austenite grains are clearly visible [Fig 3d], unlike in the case. At depths greater than 3 µm beneath the carburised surface the average grain size as characterised using the mean lineal intercept method is 50 µm ± 10 µm (ASTM 6), with a standard deviation of 20 µm between the three raceways.

Scanning electron microscopy revealed the M50NiL etching features are well-orientated parallel bands [Fig 4c]. Backscattered electron (BSE) imaging did not lead to enhanced contrast in the bands, indicating they do not differ in composition from their surroundings, [Fig 4d]. The spherical carbides in the case-carburised zone average less than 1 µm in diameter with greyscale contrast indicating species with differing average atomic number. EDX analysis confirmed V_4C_3 and Mo_2C, similar to the M50 alloy, as is consistent with [49]. The parallel bands in the M50NiL carburised case were imaged at a higher resolution using FIB-SEM [Fig 4e] and later sectioned. Many instances were identified where these structures decorated prior austenite grain boundaries [Fig 4f]. There was a shallow zone of deformation near the contact surface that was not visible optically. Used raceways sectioned in the tangential direction of rolling show evidence of significant plastic flow just 1-2 µm beneath the point of contact [Fig 4g]. This is powerful evidence of directional deformation under surface shear between components experiencing sliding contact, and within this zone a cracked carbide is identified.

Fig 5 shows TEM micrographs of the deformed band structures and the associated diffraction pattern indicating twinned martensite. Away from these regions, the general M50NiL microstructure is that of heavily dislocated martensite plates with spherical carbides and fine

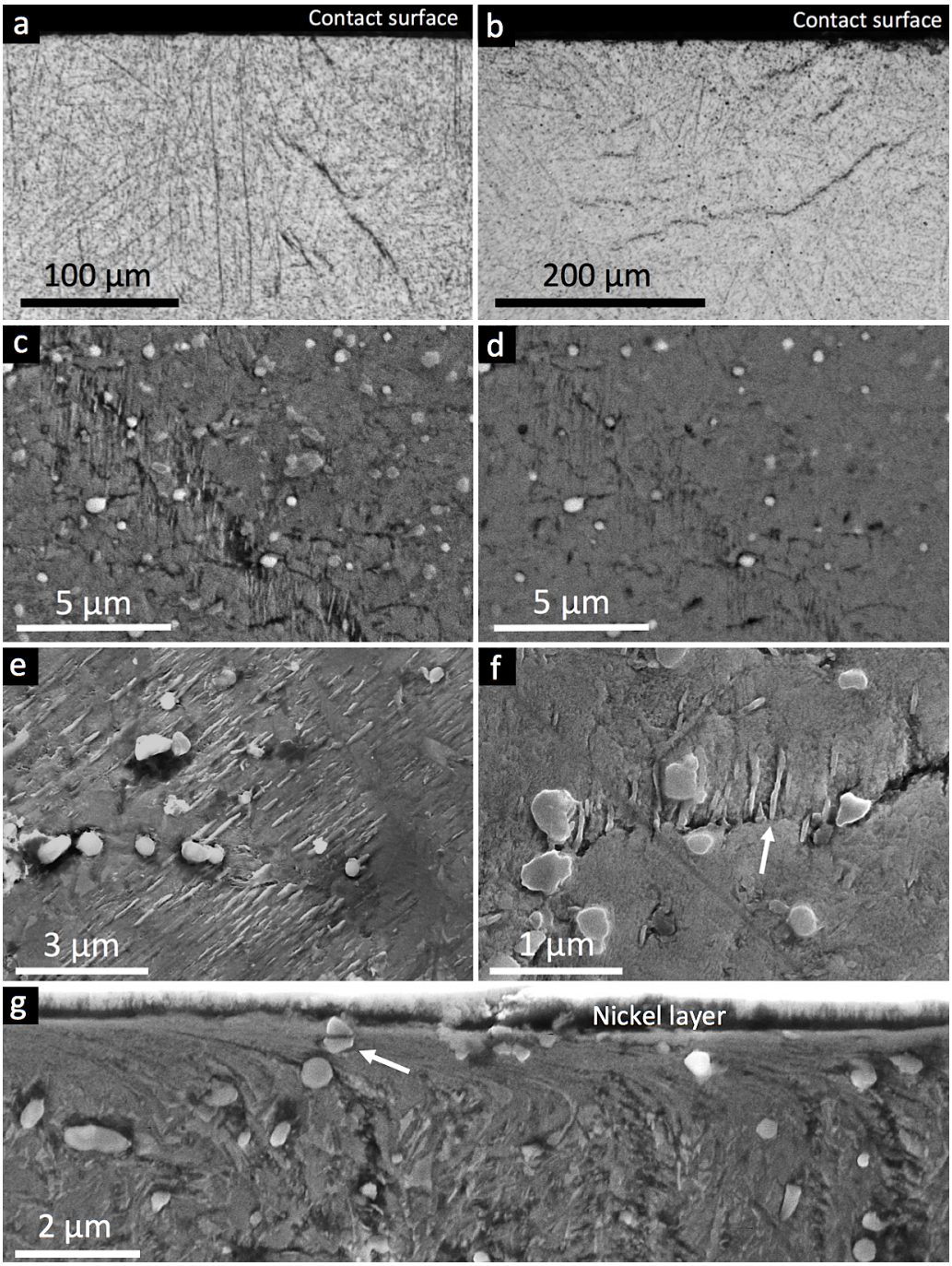

Figure 4: a). Large etching features within the carburised case of M50NiL raceways. b) The features follow irregular paths and intersect the contact surface. c). Secondary electron image of etching feature shows parallel band structures within. d). Backscatter image of same region. The bands show no compositional difference to the matrix, unlike the bright Mo_2C carbides. e). FIB-SEM image of the M50NiL bands shows their plate-like morphology. f). Plates initiate along an M50NiL prior austenite grain boundary interface (arrowed). g). Secondary electron image of the 120 h raceway shows severe plastic flow beneath the contact surface in the direction of rolling (right to left). A protective layer of nickel is deposited to protect these shallow surface features, where a cracked carbide is also located (arrowed).

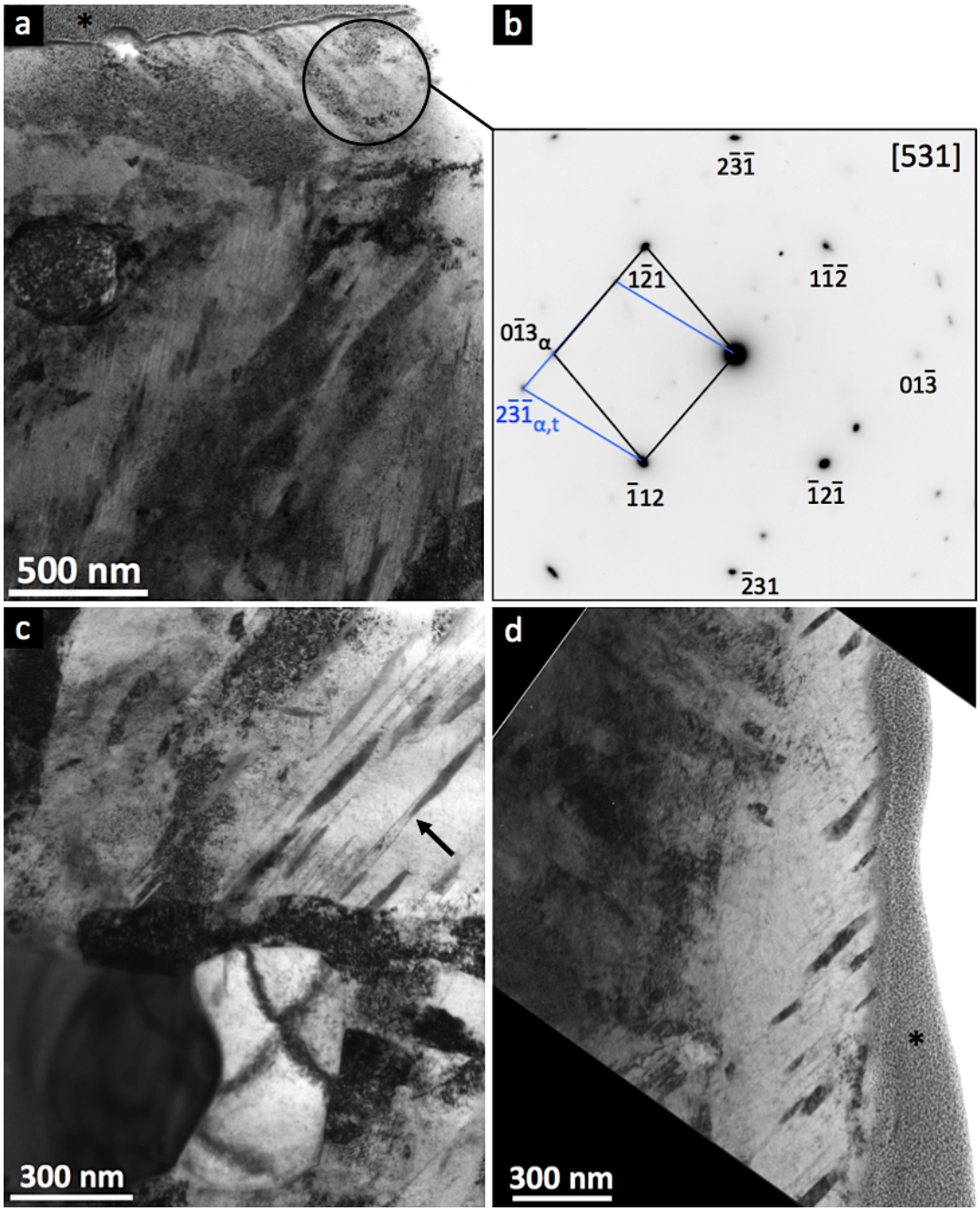

Figure 5: a). Bright field TEM micrograph of bands in the M50NiL case-carburised zone after 30,000 h service. A platinum layer* protects them during ion milling. b). Diffraction pattern of the bands showing a twinned structure. c). M50NiL case after 30,000 h service showing deformation twins with emissary dislocations at their apex. d). M50NiL case after 0 h service. This foil was taken from bands that decorated a prior austenite grain boundary [Fig 5f]. The lenticular morphology is consistent with deformation twinning.

twins. TEM foils reveal that the plate-like morphologies of the bands are consistent with deformation twins in martensite [Fig 5c], substantiated by observations of emissary dislocations produced at their apex [50]. The presence of these twins along the prior austenite grain boundary interface, as previously shown in Fig 4f, is evidence of their strain-induced nucleation. Deformation twinning is observed in the case-carburised zone of all three M50NiL raceways, indicating that service stresses are not responsible. Plastic deformation during processing and finishing of the component surfaces may be the cause. The significance of these localised, plastically-deformed regions is not clear but mechanical twinning might compromise integrity if it occurs with sufficient intensity. Such inhomogeneities in the raceway microstructure may represent defects prior to service, particularly where they intersect the contact surface [Fig 5b]. Future work should aim to quantify and ascertain whether the features become more numerous during service.

Hardness Measurement

Microhardness data on M50NiL raceways are shown in Fig 6. The 0 h raceway material shows a hardness gradient characteristic of the carburised case with values exceeding 800 HV0.2 (64 HRC) at the surface, falling to 480 HV0.2 (48 HRC) in the core material beyond 3 mm deep. The longest running of the used raceways at 30,000 h exhibited higher hardness values in the first 1 mm beneath the contact surface; peaking at 900 HV0.2 (67 HRC). Indentations made at greater depths than 1 mm tend to the same hardness gradient as the other samples, following the carburised profile of the virgin material. The intermediate service bearing raceway at 120 h displays similar hardness gradients to the 0 h raceway material.

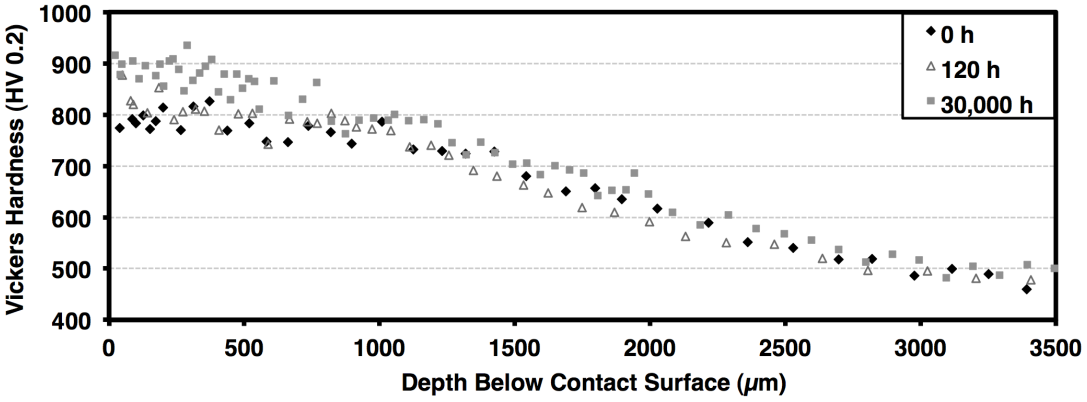

Figure 6: Vickers micro-hardness data for M50NiL aircraft gas turbine engine bearing raceways of varying service lives. A general hardness gradient is present in all cases due to carburisation and a hardness increase is apparent in the first 1 mm of the 30,000 h raceway.

A gradient in hardness is expected in the case due to the nature of the carburisation process [11]. All three raceways have similar hardness for depths >1 mm, but the increase observed in the 30,000 h race surface is indicative of work hardening under the influence of rolling contact stresses. Arakere and Subhash [51] identified work hardening in M50NiL test rods under accelerated RCF testing, attributing this to accumulated plastic strain before shakedown. Their testing was performed at much higher contact stress levels of 5.5 GPa for 10^7 fatigue cycles, compared to the present work where the contact stress remains below 2 GPa but the number of fatigue cycles accrued over 30,000 h may exceed 10^{10}. The absence of any obvious hardness increase in the 120 h raceway indicates that work hardening develops slowly with accumulated strain during prolonged rolling contact, rather than in the initial shakedown

period as is often reported in the less microstructurally stable 52100 type steels [21].

Conclusions

Microstructural features of aircraft gas-turbine engine bearing steels have been identified after time spent in service. Primary carbide segregation was observed in M50 bearing balls and a 30% reduction in their surface carbide population was identified after 30,000 h service. These carbides on the bearing ball surface give rise to raceway damage which describes sliding during rolling contact. It is this sliding shear that encourages fatigue conditions at the raceway surface, as oppose to beneath the point of contact, where the material remains in good condition. Only a shallow zone of plastic flow was identified in the direction of rolling, at depths of 1-2 µm. Etching features are encountered in the M50NiL carburised case as localised regions of mechanically twinned martensite, often found decorating prior austenite grain boundaries. This plastically deformed material is common to all three bearing raceways and so is not thought to represent fatigue damage, rather, the forming and finishing of raceway components during manufacture may be responsible. A quantitative investigation of these features is necessary to establish the significance of localised deformation twinning near the contact surface. Work hardening has been identified through an increase in Vickers hardness 1 mm beneath the point of contact after 30,000 h service, but not after 120 h service. The implication is that a gradual accumulation of strain takes place over prolonged periods of rolling contact in M50NiL, rather than an initial work hardening response during shakedown.

Acknowledgments

The authors would like to thank Rolls-Royce for their donations of full scale bearings used in this work, and would also thank Professor Lindsay Greer and Professor Mark Blamire for their provision of laboratory facilities at the Department of Materials Science and Metallurgy, University of Cambridge. Additional thanks are paid to Erik Vegter from the SKF Engineering and Research Centre, Neiuwegein for contributions and test material.

References

[1] C. Bathias. Gigacycle fatigue properties of bearing steels. *ASTM STP 1524*, pages 160–178, 2010.

[2] H. J. Bohmer, T. Hirsch, and E. Streit. Rolling contact fatigue behaviour of heat resistant bearing steels at high operational temperatures. *ASTM STP 1327*, pages 131–151, 1998.

[3] T. A. Harris, J. Skiller, and R. F. Spitzer. On the fatigue life of m50 nil rolling bearings. *Tribology Transactions*, 35(4):731–737, 1992.

[4] J. F. Braza, P. K. Pearson, and C. J. Hannigan. The performance of 52100, M-50, and M-50 NiL steels in radial bearings. *SAE Technical Paper Series*, 932470:1–13, 1993.

[5] H. Swahn, P.C. Becker, and O. Vingsbo. Martensite decay during rolling contact fatigue in ball bearings. *Metallurgical Transactions A*, 7A:1099–1110, August 1976.

[6] N. H. Forster, L. Rosado, W. P. Ogden, and H. K. Trivedi. Rolling contact fatigue life and spall propagation of AISI M50, M50NiL, and AISI 52100, Part III: Metallurgical Examination. *Tribology Transactions*, 53:52–59, 2010.

[7] B. L. Averbach and E. N. Bamberger. Analysis of bearing incidents in aircraft gas turbine mainshaft bearings. *Tribology Transactions*, 34:241–247, 1991.

[8] H. J. Bohmer. Residual stresses and material behaviour of m50nil and rbd. *ASTM STP 1195*, pages 34–48, 1993.

[9] ASTM Standard A 295-98. Specification for high-carbon anti-friction bearing steel. *ASTM International, West Conshohocken, PA*, 1998.

[10] N.K. Arakere, N. Branch, G. Levesque, V. Svendsen, and N. H. Forster. Rolling contact fatigue life and spall propagation of AISI M50, M50NiL, and AISI 52100, Part II: Stress Modelling. *Tribology Transactions*, 53:42–51, 2010.

[11] M. A. Klecka, G. Subhash, and N. K. Arakere. Microstructure-property relationships in M50-NiL and P675 case-hardened bearing steels. *Tribology Transactions*, 56(6):1046–1059, 2013.

[12] B. L. Averbach, B. Lou, P. K. Pearson, R. E. Fairchild, and E. N. Bamberger. Fatigue crack propagation in carburized high alloy bearing steels. *Metallurgical Transactions A*, 16:1253–1265, 1985.

[13] E. N. Bamberger and D. J. Kroeger. Rolling element fatigue life of a carburized modified M50 bearing steel. Final technical report, NASA, Lewis Research Centre, Ohio, 1984.

[14] K. Hirakawa, N. Ikeda, S. Okita, and A. Kiuchi. Inner ring fracture characteristics under rolling contact. *NSK Motion and Control*, 7:15–23, 1999.

[15] T. Reti. *Residual stresses in carburized, carbonitrided, and case-hardened components.* ASM International, Materials Park, OH, 2002.

[16] E. V. Zaretsky. Bearing and gear steels for aerospace applications. Technical memorandum, NASA, Lewis Research Centre, Ohio, 1990.

[17] E. N. Bamberger, B. L. Averbach, P. K. Pearson, S. Vanpeit, and M. J. Price. Improved fatigue life bearing development. Final Report AD-B137 279, Air Force Wright Aeronautical Laboratories, 1989.

[18] E. V. Zaretsky. Rolling bearing steels - a technical and historical perspective. *Materials Science and Technology*, 28:58–69, 2012.

[19] H. K. D. H. Bhadeshia. Steels for bearings. *Progress in Materials Science*, 57:268–435, 2012.

[20] F. Sadeghi, B. Jalalahmadi, T. S. Slack, N. Raje, and N. K. Arakere. A review of rolling contact fatigue. *Journal of Tribology*, 131:1–15, 2009.

[21] A. P. Voskamp. Material response to rolling contact loading. *Journal of Tribology*, 107:359–366, 1985.

[22] M. H. Evans. White structure flaking in wind turbine gearbox bearings. *Materials Science and Technology*, 28:3–21, 2012.

[23] A. Grabulov, R. Petrov, and H. W. Zandbergen. EBSD investigation of the crack initiation and TEM/FIB analyses of the microstructural changes around the cracks formed under rolling contact fatigue (RCF). *International Journal of Fatigue*, 32:576–583, 2010.

[24] Y. P. Chiu. The mechanism of bearing surface fatigue - experiments and theories. *Tribology Transactions*, 40:658–666, 1997.

[25] R. Schlatter and J. P. Stroup. Improved M50 aircraft bearing steel through advanced vacuum melting processes. *Journal of Vacuum Science and Technology*, 9(6):1326–1333, 1972.

[26] F. J. Ebert and P. Poulin. The effect of cleanliness on the attainable bearing life in aerospace applications. *Tribology Transactions*, 38:851–856, 1995.

[27] A. Tauqir, I. Salam, A. ul Haq, and A. Q. Khan. Causes of fatigue failure in the main bearing of an aeroengine. *Engineering Failure Analysis*, 7:127–144, 2000.

[28] I. Salam, A. Tauqir, A. ul Haq, and A. Q. Khan. An air crash due to fatigue failure of a ball bearing. *Engineering Failure Analysis*, 5:261–269, 1998.

[29] K. L. Johnson. *Contact Mechanics*. Cambridge University Press, 1985.

[30] Jurgen Gegner. *Tribological Aspects of Rolling Bearing Failures*. Tribology - Lubricants and Lubrication. InTech, 2011.

[31] M. J. Martin, M. P. Alanou, H. P. Evans, R. W. Snidle, H. Kawamura, and A. Dodd. Scuffing performance of m50 bearing steel lubricated was a gas turbine engine oil at high sliding speeds. *Tribology Transactions*, 44:465–471, 2001.

[32] D. Nelias, M. L. Dumont, F. Couhier, G. Dudragne, and L. Flamand. Experimental and Theoretical Investigation on Rolling Contact Fatigue of 52100 and M50 Steels Under EHL or Micro-EHL Conditions. *Transactions of the ASME*, 120:184–190, 1998.

[33] A. H. Nahm. Effect of grain flow orientation on rolling contact fatigue life of AISI M-50. *Transactions of the ASME*, 104:330–334, 1982.

[34] C. H. Hager, G. L. Doll, R. D. Evans, and P. J. Shiller. Minimum quantity lubrication of M50/M50 and M50/Si3N4 tribological interfaces. *Wear*, 271:1761–1771, 2011.

[35] P. Gloeckner and F. J. Ebert. Micro-sliding in high-speed aircraft engine ball bearings. *Tribology Transactions*, 53:369–375, 2010.

[36] D. Novovic, R. C. Dewes, D. K. Aspinwall, W. Voice, and P. Bowen. The effect of machined topography and integrity on fatigue life. *International Journal of Machine Tools and Manufacture*, 44:125–134, 2004.

[37] M. Woydt and R. Wasche. The history of the Stribeck curve and ball bearing steels: The role of Adolf Martens. *Wear*, 268:1542–1546, 2010.

[38] G. Xu and F. Sadeghi. Spall initiation and propagation due to debris denting. *Wear*, 201:106–116, 1996.

[39] A. Warhadpande and F. Sadeghi. Effects of surface defects on rolling contact fatigue of heavily loaded lubricated contacts. *Journal of Engineering Tribology*, 224:1061–1077, 2010.

[40] C. A. Schneider, W. S. Rasband, and K. W. Eliceiri. Nih image to imagej: 25 years of image analysis. *Nature Methods*, 9:671–675, 2012.

[41] A. Dodd, N. Mitamura, H. Kawamura, and Y. Ohura. Bearings for aircraft gas turbine engines (part 2). *NSK Motion and Control*, No. 6:1–8, 1999.

[42] E. V. Zaretsky. Rolling element fatigue life of ausformed M50 balls. Technical note, NASA, Washington, D.C., 1968.

[43] W. J. Anderson. Effect of fiber orientation, temperature and dry powder lubricants on rolling contact fatigue. *Tribology Transactions*, 2:108–120, 1959.

[44] T. L. Carter. A study of some factors affecting rolling-contact fatigue life. *NASA Technical Report*, R-60:1–48, 1960.

[45] J. E. Bridge, G. N. Maniar, and T. V. Philip. Carbides in M-50 high speed steel. *Metallurgical Transactions*, 2:2209–2213, 1971.

[46] P. K. Pearson and T. W. Dickinson. The role of carbides in performance of high-alloy bearing steels. *ASTM STP 987*, pages 113–131, 1988.

[47] A. Garg, T. R. McNelley, and J. L. Perry. Analysis of microporosity associated with insoluble carbides in vim-var aisi m-50 steel. *Metallography*, 20:89–98, 1987.

[48] L. Vincent, B. Coquillet, and P. Guiraldenq. Fatigue damage of ball bearing steel: Influence of phases dispersed in the martensitic matrix. *Metallurgical Transactions A*, 11A:1001–1006, 1980.

[49] D. W. Hetzner and W. V. Geertruyden. Crystallography and metallography of carbides in high alloy steels. *Materials Characterization*, 59:825–841, 2007.

[50] A. W. Sleeswyk. Emissary dislocations: Theory and experiments on the propagation of deformation twins in -iron. *Acta Metallurgica*, 10:705–725, 1962.

[51] N. K. Arakere and G. Subhash. Work hardening response of M50-NiL case hardened bearing steel during shakedown in rolling contact fatigue. *Materials Science and Technology*, 28:34–38, 2012.

Materials Science and Technology 30 (2014) 1911-1918